Engineering vortex rings and systems for controlled studies of vortex interactions in Bose-Einstein condensates

Janne Ruostekoski[1,2] and Zachary Dutton[3]
[1]*School of Mathematics, University of Southampton, Southampton SO17 1BJ, United Kingdom*
[2]*Department of Physics, Astronomy and Mathematics, University of Hertfordshire, Hatfield, Herts AL10 9AB, United Kingdom*
[3]*Naval Research Laboratory, Washington, D.C. 20375, USA*
(Received 5 June 2005; published 30 December 2005)

We study controlled methods of preparing vortex configurations in atomic Bose-Einstein condensates and their use in the studies of fundamental vortex scattering, reconnection processes, and superfluid sound emission. We explore techniques of imprinting vortex rings by means of coherently driving internal atomic transitions with electromagnetic fields which exhibit singular phase profiles. In particular, we show that a vortex ring can be prepared by two focused co-propagating Gaussian laser beams. More complex vortex systems may also be imprinted by directly superposing simpler field configurations or by programming their phase profiles on optical holograms. We analyze specific examples of two merging vortex rings in a trapped two-species ^{87}Rb gas. We calculate the radiated sound energy in the reconnection process and show that the vortex relaxation and the redistribution of sound energy can be controlled by the imprinting process. As another creation technique, we study engineering pairs of two-dimensional point vortices in the condensates using a 'light roadblock' in ultraslow light propagation. We show how this can be used to study vortex collisions in compressible superfluids and how these collisions result in energy dissipation via phonons and, sometimes, annihilation of vortex pairs.

DOI: 10.1103/PhysRevA.72.063626 PACS number(s): 03.75.Kk, 03.75.Lm, 03.75.Mn, 67.40.Vs

I. INTRODUCTION

One of the advantages of atomic Bose-Einstein condensates (BECs), as compared to more traditional quantum fluids, is the dramatic flexibility of experimental preparation. Both the internal and the center-of-mass states of ultracold atoms can be manipulated and controlled in diverse ways using electromagnetic (em) fields. In this paper we explore the possibilities of using the present day atomic physics technology as a sophisticated state engineering tool, in order to construct highly nontrivial superfluid states in atomic many-particle systems. In particular, such a 'field-theory engineering' may be useful in preparing topological defects, studying their interactions, and the decay of superfluid turbulence [1]. We consider controlled methods of creating vortex systems by means of directly imprinting phase singularities on the BECs from em fields and by means of inducing density defects via the ultraslow light propagation inside the BEC. In the case of the phase imprinting techniques, we focus on the preparation of vortex rings and we show, as an example, how the method could be applied to the studies of the time evolution and the reconnection process of two merging vortex rings. For the case of ultraslow light propagation we demonstrate, again by numerical examples, how it can be employed in the studies of the collision of point vortex pairs and their sound emission.

In the phase imprinting process we consider em field configurations which exhibit phase singularities in the field amplitude. When such a field is used to drive internal atomic transitions, the nonuniform phase profile of the em field amplitude may be imprinted on the matter wave, resulting in a topologically nontrivial phase profile in the atomic condensate. We show how a reasonably simple em field configuration of two phase-coherent Gaussian laser beams could be used to imprint a vortex ring in atomic BECs by simultaneously controlling the position, the orientation, and the radius of the ring. More complex vortex structures, such as knotted vortex lines, may be imprinted using optical holograms.

Moreover, we study in detail the application of this technique to the imprinting of a pair of vortex rings and study their reconnection dynamics in a trapped two-component ^{87}Rb condensate, using experimentally feasible parameters. Such reconnections have escaped experimental observation in BECs to date. The two rings merge together and the resulting turbulent dynamics generate an effective local dissipation in the gas, allowing the vortex configuration to relax to lower energy without an explicit damping term in the dynamics. This mechanism is also analogous to the dynamical formation of a vortex lattice in a rotating zero temperature BEC [2]. We qualitatively analyze the redistribution of sound energy in the trapped cloud due to the vortex reconnection processes. The energy is first concentrated towards the trap center and later emitted outwards as sound and transformed to surface excitations. Here the excitation of kelvin waves and the radiated sound energy can be controlled by changing the parameters of the em fields. Although vortex rings, as localized singular defects which are detached from superfluid boundaries, are interesting in their own right, they can also form a building block of energetically stable localized particle like solitons [three-dimensional (3D) Skyrmions] in a two-component ^{87}Rb BEC [3–5], providing a link between ultracold atom physics, elementary particles, and cosmology.

As another method of engineering systems for studying fundamental vortex interactions, we consider the generation of a 'light roadblock' [6] by abruptly distorting the ultraslow

light propagation [7–9] in a BEC. The strong nonlinear coherent light-matter coupling is based here on the method of electromagnetically induced transparency (EIT) [10], which allows propagation of light pulses through the BEC due to the lack of absorption. If the probe and the coupling beams are propagating in orthogonal directions and the coupling field is varied quickly to zero over a short distance near the BEC center, the probe field is abruptly compressed and stopped inside the atom cloud. This results in a large transfer of atom population between the internal states and the emergence of a very narrow density defect inside the BEC, which subsequently generates solitons via quantum shock waves [6] and then vortex pairs via the snake instability [11–13]. In Ref. [14] it was noted that this can be used to create a "gas" of multiple vortex particles, of both circulations, which are out of equilibrium and subsequently interact. Here we show that in a 2D geometry the generation of the defects can be controlled to yield desired configurations of point vortex pairs whose collisions and sound emission can be investigated in detail. In order to demonstrate the usefulness of the preparation scheme we analyze some sample cases of point vortex pair creation and the resulting vortex collision dynamics. In particular, we focus on a regime in which the size of the vortex pairs is comparable to the healing length in the superfluid. In such a case, collisions of vortex pairs are more complicated than they are in the incompressible limit [15], as the collisions can cause energy to be dissipated in the form of phonons. This dissipation alters the collision dynamics and can lead to annihilation of vortex pairs, another interesting phenomenon which has hitherto been unobserved experimentally. We present a numerical study of this and show how the light roadblock may allow its observation.

The quantized vorticity in atomic superfluids has inspired considerable experimental and theoretical activity in recent years [16]. There have been several theoretical proposals to imprint vortex line singularities on atomic BECs by means of transferring angular momentum on atoms from em fields [17–25] and some of the techniques have already been experimentally realized [26–29]. In Ref. [26], a vortex line with one unit of circulation was imprinted on a pair of condensates occupying different internal levels of ^{87}Rb using a Raman coupling which was set locally resonant in a small region by rapidly rotating laser beams. In Refs. [27–29], singular singly quantized and doubly quantized, as well as nonsingular coreless vortex lines were created by adiabatically inverting the magnetic bias field along the trap axis. Also dark solitons have been imprinted on atomic BECs, e.g., by imaging the atom cloud through an absorption plate [30,31]. Such π phase kink planes have been observed to decay into a hybrid of vortex rings and lines through the dynamical "snake" instability [6,13,32]. A controlled method of creating vortex rings and particlelike solitons was proposed in Ref. [3], where it was shown that a topological phase singularity forming a closed circular loop may be imprinted on the matter field while changing the internal state of the atoms. Ring defects in spinor BECs may also form from simpler core structures as a result of dissipation [33]. The defect generation using a light roadblock was realized in Ref. [6]. More complicated defect configurations were recently produced by superposing multiple roadblocks [32]. It has also been proposed that the strong light-matter coupling of the ultraslow and stopped light [34–36] could be used to efficiently transfer vortex states between light and atomic BECs and to store light modes with orbital angular momentum inside the BECs [25], as well as to use a vortex lattice to create a photonic band gap [37].

In Sec. II we show how em fields containing phase singularities can be used to imprint vortex rings on BECs. We discuss several examples of how the required fields can be generated by superpositions of plane and/or Gaussian laser fields. In Sec. III we apply the method to generate two vortex rings and to study their ensuing reconnection dynamics. In Sec. IV we then turn using the light roadblock to generate systems of multiple vortex point particles in a 2D geometry, focusing on collisions of vortex pairs, which dissipate energy via phonons and sometimes leads to vortex annihilations.

II. CONTROLLED PREPARATION OF VORTEX RINGS

A. Coupled two-component condensate

A vortex ring can be engineered by using an em field to imprint topological phase singularities on the matter field while changing the internal state of the atoms [3]. Here we consider a two-component BEC where the two internal states are coupled by means of the em fields with the Rabi frequency $\Omega(\mathbf{r})$. The dynamics of the BECs with the Rabi coupling between the levels $|i\rangle$ and $|j\rangle$ follow from the coupled Gross-Pitaevskii equation (GPE):

$$i\hbar\frac{\partial\psi_i}{\partial t}=\left(H_0+\delta_i+\sum_k\kappa_{ik}|\psi_k|^2\right)\psi_i+\hbar\,\Omega^*\psi_j. \tag{1}$$

We assume the two-component condensate, with the total number of N atoms and the atomic mass m, to be confined in a perfectly overlapping, isotropic trap with the trap frequency ω:

$$H_0\equiv-\frac{\hbar^2}{2m}\nabla^2+\frac{1}{2}m\omega^2r^2. \tag{2}$$

The parameter $\delta_j(\mathbf{r})$ incorporates the detuning of the em fields from the resonance of the internal transition as well as em field-induced level shifts which may be nonuniform in the case of a spatially varying field intensity. We have also defined the interaction coefficients $\kappa_{ij}\equiv 4\pi\hbar^2a_{ij}N/m$, with the intraspecies and the interspecies scattering lengths denoted by a_{ii} and a_{ij} $(i\neq j)$, respectively. Such a system has been experimentally realized using, e.g., the $|2\rangle\equiv|S_{1/2},F=2,M_F=+1\rangle$ and $|1\rangle\equiv|S_{1/2},F=1,M_F=-1\rangle$ hyperfine spin states of ^{87}Rb. The two hyperfine levels were coupled by means of a two-photon transition (one microwave and one rf photon). For the ^{87}Rb components the interaction strengths are nearly equal, with $a_{11}:a_{21}:a_{22}::1.03:1:0.97$ and $a_{21}\simeq 5.50$ nm [38]. Since the scattering lengths satisfy $a_{21}^2\gtrsim a_{11}a_{22}$, the two species experience dynamical phase separation and can strongly repel each other [38]. In the absence of the em coupling between the different components the interatomic interactions of the two ^{87}Rb components do not

mix the atom population and the atom numbers of both species are separately conserved.

The phase profile of the driving em field can be imprinted on the matter wave by means of transferring the atomic population between the two different internal levels. We assume that all the BEC atoms initially occupy one of the hyperfine states, let us say $|2\rangle$. Some population is then transferred from $|2\rangle$ to $|1\rangle$ by means of a Rabi pulse $\Omega(\mathbf{r},t)$. After the pulse, the relative phase between the BECs in the two levels is proportional to the phase profile of the Rabi field, as indicated by Eq. (1). We may construct a phase profile for the em field, where the node points of the field amplitude may correspond to the topological singularities of the phase of the em field. The em coupling provides then a method for imprinting these topological singularities on the condensate. In order to imprint a vortex ring on the $z=0$ plane, centered at the z axis, we require the em field to exhibit a closed circular phase singularity in such a way that in the close neighborhood of the circular node the field is of the form

$$\Omega(\mathbf{r},t) \simeq \mathcal{R}(t)[(\rho-\rho_0)+i\gamma z] = \mathcal{R}(t)\,\eta e^{i\theta}, \tag{3}$$

where $\rho \equiv (x^2+y^2)^{1/2}$ and ρ_0 denotes the radius of the ring. Here we have also defined $\eta \equiv [(\rho-\rho_0)^2+\gamma^2 z^2]^{1/2}$ and $\theta \equiv \arctan[\gamma z/(\rho-\rho_0)]$. The field amplitude (3) vanishes at the ring $(\rho=\rho_0, z=0)$ with the desired 2π phase winding along any closed loop encircling the ring, representing one unit of quantized circulation around the ring. The parameter γ describes the anisotropy of the vortex core and $\gamma=1$ corresponds to an isotropic core. Once the phase is imprinted on the BEC, the superfluid velocity of the atoms is obtained from

$$\mathbf{v}(\mathbf{r}) = \frac{\hbar}{m}\nabla\,\theta, \tag{4}$$

and the parameter γ also determines the anisotropy of the velocity field. For instance, close to $x \simeq \rho_0$, we have $\mathbf{v}(x, y=0, z=0) \simeq \gamma/(x-\rho_0)\hat{\mathbf{e}}_z$ and $\mathbf{v}(x=\rho_0, y=0, z) \simeq 1/(\gamma z)\hat{\mathbf{e}}_x$. The condensate excitations are reduced for the case of an isotropic core $\gamma=1$.

B. Imprinting a vortex ring

A technique to imprint a vortex ring on the BEC was proposed in Ref. [3] by means of constructing an em field amplitude which exhibits the desired form (3). This was obtained using

$$\Omega(\mathbf{r}) = \Omega_0[\alpha - f(x,y) + i\beta\sin(kz)], \tag{5}$$

Here the Rabi amplitude represents a coherent superposition of a standing wave along the z axis, a constant field α, and the field $f(x,y)$, which could be a Gaussian field focused weakly on the xy plane or, alternatively, a superposition of two standing waves along the x and the y directions:

$$f(x,y) = \exp\left(-\frac{\rho^2}{\xi^2}\right), \tag{6}$$

$$f(x,y) = \frac{1}{2}\left(\cos\frac{2x}{\xi} + \cos\frac{2y}{\xi}\right). \tag{7}$$

We assume $\rho/\xi \sim \sqrt{1-\alpha} \ll 1$. Then by expanding Eqs. (5) and (7) to first order in ρ/ξ and $k|z| \ll 1$, we obtain Eq. (3) with $\rho_0 = \xi\sqrt{1-\alpha}$ and $\gamma = \beta\xi^2 k/2\rho_0$. Hence, a constant field with three orthogonal standing waves, or, alternatively, with a standing wave and a parallel Gaussian beam, are sufficient to imprint a vortex ring on an atomic BEC. Moreover, this results in an isotropic vortex core with $\gamma=1$ when we choose $\alpha = 1-(\beta\xi k/2)^2$.

The field configuration (5) is most suitable for microwave (or longer wavelength) em fields for which the wavelength $\lambda = 2\pi/k$ is longer than the typical radius R of the BEC. For optical fields $\lambda < R$ the em coupling would create multiple copies of the ring, displaced from each other by $\lambda/2$. However, even for optical fields it should be possible to shape the wave fronts of the coupling lasers in order to avoid rapid phase variation at the length scale λ. This could be done, e.g., by using microlens arrays [39], laser beams copropagating in the direction of the standing wave z, or beams with the wave vectors nearly perpendicular to z. Here we show that another alternative is to consider two-photon transitions via some intermediate level $|3\rangle$ and use slightly different wave numbers for the lasers. Consider the first transition $|2\rangle \to |3\rangle$ to be induced by four copropagating laser beams, one of which is weakly focused on the xy plane,

$$\Omega_2(\mathbf{r}) = \bar{\Omega}_2\left[(\alpha - e^{-\rho^2/\xi^2})e^{ikz} + \frac{\beta}{2}(e^{i(k+k')z} - e^{i(k-k')z})\right]. \tag{8}$$

Here we assume that $k' \ll k$ and the coupling frequency $\Omega_2 = \mathbf{d}_{23}\cdot\mathbf{E}_2^+/\hbar$ is in this case determined in terms of the atomic dipole matrix element $\mathbf{d}_{23}$ of the transition $|2\rangle \to |3\rangle$ and the positive frequency component of the driving electric field $\mathbf{E}_2^+$. The second transition $|3\rangle \to |1\rangle$ is driven by a nonfocused copropagating field $\Omega_1(\mathbf{r}) = \bar{\Omega}_1 \exp(ikz)$, which cancels the rapid phase variation of Ω_2 along the z axis. In the limit of large detuning Δ of the laser $\Omega_2(\mathbf{r})$ from the resonance of the $|2\rangle \to |3\rangle$ transition, the effective Rabi frequency for the $|2\rangle \to |1\rangle$transition then reads

$$\Omega_{21}(\mathbf{r}) \simeq \frac{2\Omega_2(\mathbf{r})\Omega_1^*(\mathbf{r})}{\Delta} = \frac{2\bar{\Omega}_2\bar{\Omega}_1^*}{\Delta}[\alpha - e^{-\rho^2/\xi^2} + i\beta\sin k'z]. \tag{9}$$

This has the desired form (5). In addition, even though we may have $kR \gg 1$, it should be possible to choose $k' \ll k$, so that $k'R \lesssim 1$. This allows us to create precisely one vortex ring in the BEC.

In a more challenging scheme, one may construct an optical lattice with a long periodicity [19] by means of superposing two separate two-photon transitions

$$\sin[(k_1-k_2)z] = \frac{1}{2i}(e^{ik_1 z}e^{-ik_2 z} - e^{-ik_1 z}e^{ik_2 z}), \tag{10}$$

such that $(k_1-k_2)R \lesssim 1$. Here each exponent factor represents a running wave transition by one photon.

In the following, we demonstrate how the vortex ring could also be imprinted using only two Gaussian laser beams providing an experimentally simple scheme for a controlled creation of vortex rings.

C. Imprinting a vortex ring using Gaussian beams

Here we show that a vortex ring defect can also be imprinted on an atomic BEC in a controlled way by means of two parallel Gaussian laser beams. The advantage of this scheme, as compared, e.g., to Eq. (8) is the obvious simplicity of the field configuration and the common experimental availability of the beams. The complete expression of the Gaussian laser beam reads

$$\mathcal{G}(\mathbf{r},w_0) = \frac{w_0}{w(z)} \exp\left[ikz - i\arctan\frac{z}{z_0} + ik\frac{\rho^2}{2R(z)}\right] \times \exp\left[-\frac{\rho^2}{w(z)^2}\right], \tag{11}$$

where $w(z) \equiv w_0\sqrt{1+z^2/z_0^2}$ and $R(z) \equiv z(1+z_0^2/z^2)$. Here w_0 represents the minimum beam waist and $z_0 \equiv \pi w_0^2/\lambda$ is the Rayleigh range, the distance over which the focusing is increased to $\sqrt{2}w_0$ due to diffraction. In a weakly focused beam, for $\rho \ll w_0$, $|z| \ll z_0$, $\mathcal{G}(\mathbf{r},w_0) \simeq \exp(ikz - \rho^2/w_0^2)$.

We take the two Gaussian beams as a phase-coherent superposition:

$$\Omega_r(\mathbf{r}) = \Omega_0[\mathcal{G}(\mathbf{r},w_0) + c\mathcal{G}(\mathbf{r},w_0')], \tag{12}$$

for some complex c. It is straightforward to see that by choosing

$$c = -\exp\left[-\rho_0^2\left(\frac{1}{w_0^2} - \frac{1}{w_0'^2}\right)\right], \tag{13}$$

the field configuration (12) exhibits a circular node at $(\rho=\rho_0, z=0)$ with the 2π phase winding around the ring. The complete destructive interference of the two Gaussian beams does not occur outside the plane of the minimum beam focus size due to diffraction. By modifying the relative amplitude and the focusing of the beams, the size of the ring can be changed in a controlled way. The anisotropy of the core is determined by

$$\gamma = \frac{w_0^2 w_0'^2 - (w_0^2 + w_0'^2)\rho_0^2}{w_0^2 w_0'^2 \rho_0 k}. \tag{14}$$

In order to avoid the rapid phase variation of the Gaussian laser along the z axis to be imprinted on the BEC, it is again advantageous to consider a two-photon transition via some intermediate level $|3\rangle$ using copropagating lasers, so that, e.g., the field $\Omega_r(\mathbf{r})$ in Eq. (12) drives the transition $|2\rangle \rightarrow |3\rangle$ and a nonfocused copropagating field $\Omega_{31}\exp(ikz)$ drives the transition $|3\rangle \rightarrow |1\rangle$. In the limit of large detuning Δ, the effective Rabi frequency for the $|2\rangle \rightarrow |1\rangle$ transition then reads $2\Omega_{31}\Omega_r(\mathbf{r})\exp(-ikz)/\Delta$. The corresponding spatially nonuniform laser-induced level shifts are $\delta_1(\mathbf{r}) \simeq 2|\Omega_{31}(\mathbf{r})|^2/\Delta + \delta_{12}$ and $\delta_2(\mathbf{r}) \simeq 2|\Omega_r(\mathbf{r})|^2/\Delta$, where δ_{12} is the effective two-photon detuning from the resonance of the internal transition $|2\rangle \rightarrow |1\rangle$.

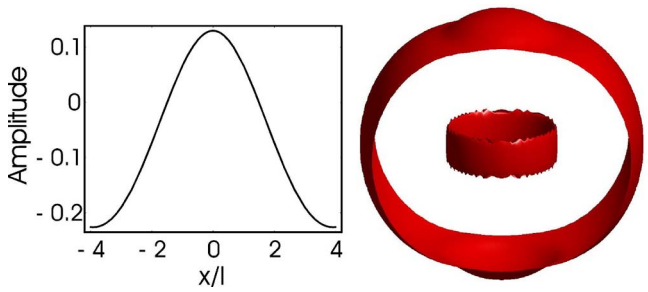

FIG. 1. (Color online) The amplitude of the superposition of two Gaussian laser beams at $z=0$ (on the left). The cylindrically symmetric amplitude exhibits a node point at $\rho_0 = 1.5l$. The constant surface plot of a vortex ring in an atomic BEC (on the right) with the phase profile imprinted from the two Gaussian laser beams. The Rabi frequency $\propto e^{-ik_2 z}\Omega_r$. Here the beam parameters are $w_0 = 3.0l$, $w_0' = 4.5l$, $kl = 7$, $k_2 l = 6.86$, and the radius of the ring $\rho_0 = 1.5l$. As a result of the imprinted phase pattern, the vortex ring slowly moves along the beam axis.

In Fig. 1 we show an example of a vortex ring in a two-component BEC, obtained by imprinting the phase profile of the two Gaussian laser beams from Eq. (12). We use the parameters of ^{87}Rb with the nonlinearity $\kappa_{21} = 500\hbar\omega l^3$ and the radius of the ring $\rho_0 = 1.5l$, where $l = \sqrt{\hbar/m\omega}$. The ring occupies the level $|1\rangle$ with the atom numbers $N_2/N_1 \simeq 6.2$. For the chosen parameters, the vortex core is noticeably anisotropic with $\gamma \simeq 0.06$. A more isotropic core, and a less excited vortex, may be obtained, e.g., by decreasing the radius of the ring by means of changing the value c according to Eq. (13). For $\rho_0 = 1.0l$ we obtain $\gamma \simeq 0.12$ and for $\rho_0 = 0.5l$, $\gamma \simeq 0.27$. As a result of the nonlinear evolution and dissipation, an anisotropic vortex core in an atomic BEC is generally expected to relax towards an isotropic core shape.

Experimentally, one could prepare the phase-coherent field configuration (12) using a single laser source which is split in two and later recombined after appropriately modifying the relative amplitude and the beam focusing. One possible experimental limitation might then be a slight misalignment of the two recombined Gaussian beams. We also tried field configurations with the propagating axes of the two beams displaced. It is quite easy to show that the vortex ring singularity Eq. (12) is robust against perturbations where the two Gaussian beams are slightly modified.

D. Multibeam superpositions

Two beam configurations, such as Eq. (12), or more complicated multibeam superpositions can also be prepared using diffractive optical components. In particular, computer-generated holograms and spatial light modulators may be used to prepare the desired optical field superpositions which are required to imprint the vortices on the atomic BECs. By using a third Gaussian beam in Eq. (12) we may better optimize the field parameters according to a steady-state vortex ring solution, or, alternatively, to engineer some desired excitations in the ring. With the superposition:

$$\Omega_r(\mathbf{r}) = \Omega_0[\mathcal{G}(\mathbf{r},w_0) + c_1\mathcal{G}(\mathbf{r},w_1) + c_2\mathcal{G}(\mathbf{r},w_2)], \tag{15}$$

we may, e.g., choose the parameters c_1 and c_2 according to the given vortex ring radius and the core isotropy, while w_0,

w_1, and w_2 may be optimized to determine the spatial profile of the BEC wave function.

E. Knotted vortex lines

More complicated field superpositions than the one shown in Eq. (15) have been successfully created using spatial light modulators. In Refs. [40,41] a field configuration of four optical Laguerre-Gaussian beams, with each exhibiting zero, one, or two units of orbital angular momentum, were generated using a liquid crystal array acting as a phase mask and controlling both the field amplitude and the phase. Such a field superposition possesses a phase singularity forming a closed knotted loop [42,43] (a torus knot) in a paraxial field and, in principle, could also be imprinted inside a BEC, provided that the hologram has a sufficient spatial resolution in order to allow the beams to be focused inside the atomic cloud.

III. ENGINEERING VORTEX RECONNECTIONS

A. Preparing multiple vortex rings

We may also use the techniques described in the previous section to imprint multiple vortex rings on the BEC. Generally this can be done by using multiphoton transitions, where the effective Rabi pulse is of the form

$$\Omega(\mathbf{r},t) \simeq \mathcal{R}(t)\prod_{j=1}^{n}[(\rho^{(j)}-\rho_0^{(j)})+i(z^{(j)}-z_0^{(j)})]^{p_j}, \qquad (16)$$

where we write $\rho^{(j)}=[(x^{(j)}-x_0^{(j)})^2+(y^{(j)}-y_0^{(j)})^2]^{1/2}$, representing n vortex rings on the plane $z^{(j)}=0$, centered at $(x^{(j)}=x_0^{(j)}, y^{(j)}=y_0^{(j)}, z^{(j)}=z_0^{(j)})$, with the radius given by $\rho_0^{(j)}$. All the vortex rings in Eq. (16) do not need to have the same orientation, but the axis $\mathbf{r}^{(j)}$ may involve different spatial rotations with respect to some fixed axis $\mathbf{r}$. The exponent p_j in Eq. (16) denotes the topological charge of the vortex ring j.

We numerically studied the preparation of two nonoverlapping vortex rings by integrating the coupled GPE (1) in the presence of the em coupling. In Fig. 2 we show an example of two vortex rings with the radii $\rho_0=0.9l$ prepared on the $z=0$ plane. Both rings are displaced from the trap center in opposite directions by $1.5l$. Here the vortex rings are created by means of the em field $\Omega(\mathbf{r}-\mathbf{r}_1)\Omega(\mathbf{r}-\mathbf{r}_2)$ (for $\mathbf{r}_1=-\mathbf{r}_2=1.5l\hat{y}$) with $\Omega(\mathbf{r})$ determined by Eqs. (5) and (6) The wavelength $\lambda=26l$, $\beta\simeq 8.3\times 10^{-3}$, and the width $\xi=30l$. We use the parameters of ^{87}Rb with the atoms initially occupying the level $|2\rangle$. The nonlinearity is $\kappa_{21}=430\hbar\omega l^3$. A short pulse $t\omega=0.1$ is applied to transfer population to the level $|1\rangle$ in order to prepare the vortex rings. This could be, e.g., a two-photon transition via some intermediate level $|3\rangle$, where the field $\Omega(\mathbf{r}-\mathbf{r}_1)$ drives the transition $|2\rangle\rightarrow|3\rangle$ and the field $\Omega^*(\mathbf{r}-\mathbf{r}_2)$ drives the transition $|3\rangle\rightarrow|1\rangle$. Alternatively, we could have used the Gaussian laser beams (12), e.g., driving a two-photon Λ three-level transition, where the beams inducing the second transition are copropagating with the first pair of beams, but are multiplied by the phase factor (-1) and displaced in space by the amount of $3l$. By modifying the strength and the duration of the Rabi pulse we can control the excitation of the vortex ring pair. This allows us to study the dynamics of the vortex ring interactions for different initial conditions.

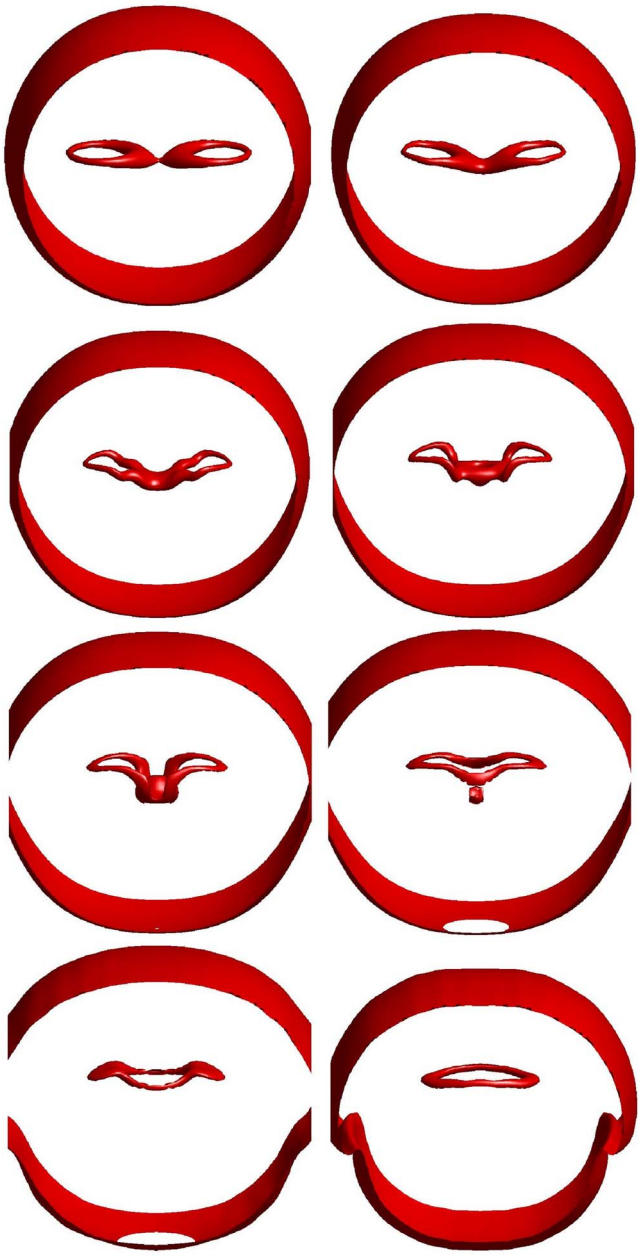

FIG. 2. (Color online) The snapshot images of the isosurface plots during the time evolution of two merging vortex rings in a trapped two-component BEC. We show the BEC component containing the two vortex rings, while the other component exhibits a uniform phase profile. The initial state was prepared by means of an em coupling field between the two BEC components, which imprints the desired phase singularities on the matter field while changing the internal level of the atoms. In order to relax the energy of the initial state, we integrated the wave functions in imaginary time for the duration of $t\omega=0.06$ before the real time evolution. We show the isosurface plots at times $t\omega=0.1$, 0.2, 0.3, 0.4, 0.5, 0.6, 1.0, and 1.4.

B. Vortex ring reconnections

Vortex reconnections represent basic vortex-vortex interactions. These are of fundamental interest in their own right, as well as providing a useful model to investigate superfluid turbulence which can be considered as being due to the dynamics of a dense tangle of quantized vortex filaments [1]. The evolution of such a tangle crucially depends on the vortex reconnections. The vortex reconnections also have an analogy with the models describing the evolution of cosmic strings in the early Universe cosmology [44]. At very low temperatures, with negligible normal fluid fraction, the superfluid turbulence and the vorticity is expected to decay as a result of sound emission [45]. Sound emission may occur due to the vortex motion or reconnection.

The proposed techniques of vortex imprinting provide a useful tool in investigating vortex reconnections in superfluids. Atomic BECs can be cooled down to very low temperatures with negligible normal fluid component. By modifying the pulse parameters of the imprinting process we may also control the level of excitation in the system. Moreover, vortices in two-component BECs offer several additional advantages. First, it is possible to monitor the system in real time: The filling of the vortex cores by the other BEC significantly increases the core size, as compared to vortices in a single-component BEC, and makes them observable *in situ*, even without a ballistic expansion. Second, the nonlinearity of the vortex excitations can be easily controlled by varying the relative density in the two components (via the strength and the duration of the coupling laser fields).

The vortex reconnections have previously been numerically studied using the GPE for the parallel and crossed line vortices [46,47] and for colliding vortex rings [48,49] in a homogeneous single-component BEC. In Refs. [48,49] two vortex rings with an initial relative velocity were scattered from each other, varying the angle of intersection and the impact parameter. As a result, a substantial loss of vortex line length was observed, which was attributed to sound emission.

As an application of the multiring imprinting techniques, we have shown here how to create two initially static vortex rings in a trapped inhomogeneous two-component BEC, which will later interact and collide. The two vortex rings on the same $z=0$ plane were imprinted using em fields, as explained in the previous section. Due to the filling of the vortex core by the second BEC component, an isolated vortex ring would approximately remain in the same location in the trap on the time scale of the trap period. If the initial separation of the rings is sufficiently small, the vortex rings are attracted to each other and merge locally, after the em coupling fields have been turned off.

Qualitatively, the long-range interaction energy between vortex filaments s and s' with the vorticity κ and κ' may be obtained, analogously to the magnetostatics, from [50]

$$E = \frac{n\kappa\kappa'}{8\pi} \int \frac{d\mathbf{s}\cdot d\mathbf{s}'}{|\mathbf{r}(s)-\mathbf{r}(s')|}. \tag{17}$$

Two antiparallel vortex filaments are attracted to each other. Once the vortex cores are close enough, they merge at the point of the closest approach. Since the facing segments of the two similarly circulating rings on the same plane represent vorticity with the opposite circulations, these segments are attracted to each other and eventually they annihilate. Consequently, the two rings are joined together. By integrating Eq. (17) with an appropriate cut-off, we may also obtain the energy of an isolated vortex ring as $E \propto n\rho_0[\ln(\epsilon\rho_0)-2]$, where n denotes the density and the parameter ϵ depends, e.g., on the core thickness [47,51] and where ρ_0 denotes the ring radius. Close to equilibrium the reduction of the vortex core length can indicate the emitted sound energy [52].

In the numerical studies of the two-component BEC dynamics, we use initial states corresponding to different strengths of excitation. These could be created by changing the strength and the duration of the em pulse in the imprinting process. However, for computational simplicity, here we always use the same pulse parameters, but relax the initial state by means of varying length of imaginary time evolution before the actual dynamics.

In Figs. 2 and 3 we show the snapshot images of the real time evolution of the two vortex rings after they were prepared by means of the Rabi coupling, as explained in the previous section. The images were obtained by numerically solving the coupled GPE (1) for the trapped two-component BEC in the absence of the coupling fields Ω. The integration was performed using the split-step method [53] on a spatial grid of 128^3. The 3D mean-field dynamics correspond to the parameters of ^{87}Rb experiments, as described in the previous section. The number of atoms in the two components $N_2 \simeq 0.86N$ and $N_1 \simeq 0.14N$, where the total atom number $N = 430l/(4\pi a_{12})$.

In Fig. 2 the initial state, obtained from the numerical integration of the Rabi coupling, was relaxed by means of imaginary time evolution of duration $t\omega = 0.06$ before the displayed real time evolution. In Fig. 3 the initial imaginary time evolution was $t\omega = 0.02$ and the merging process of the two rings is more violent. During the imaginary time evolution we separately normalized both wave functions ψ_1 and ψ_2, corresponding to the separate conservation of the atom number in each BEC component in the absence of the coupling field. We also show the total condensate energy density ϵ_t, averaged over the spherical angles,

$$\epsilon_t(r) \equiv \frac{1}{4\pi} \int d\varphi\, d(\cos\theta) \sum_{ij=1,2} \psi_i^* \left(H_0 + \frac{\kappa_{ij}}{2}|\psi_j|^2 \right) \psi_i, \tag{18}$$

as a function of the BEC radius and evolution time in Fig. 4 for the cases shown in Figs. 2 and 3, as well as for cases without the initial imaginary time evolution and for the imaginary time propagation of duration $t\omega = 0.1$. In Fig. 5 we show the contribution ϵ_1 to the energy density which only depends on the atom density in the component $|1\rangle$ containing the vortex rings:

$$\epsilon_1(r) \equiv \frac{1}{4\pi} \int d\varphi\, d(\cos\theta) \psi_1^* \left(H_0 + \frac{\kappa_{11}}{2}|\psi_1|^2 \right) \psi_1. \tag{19}$$

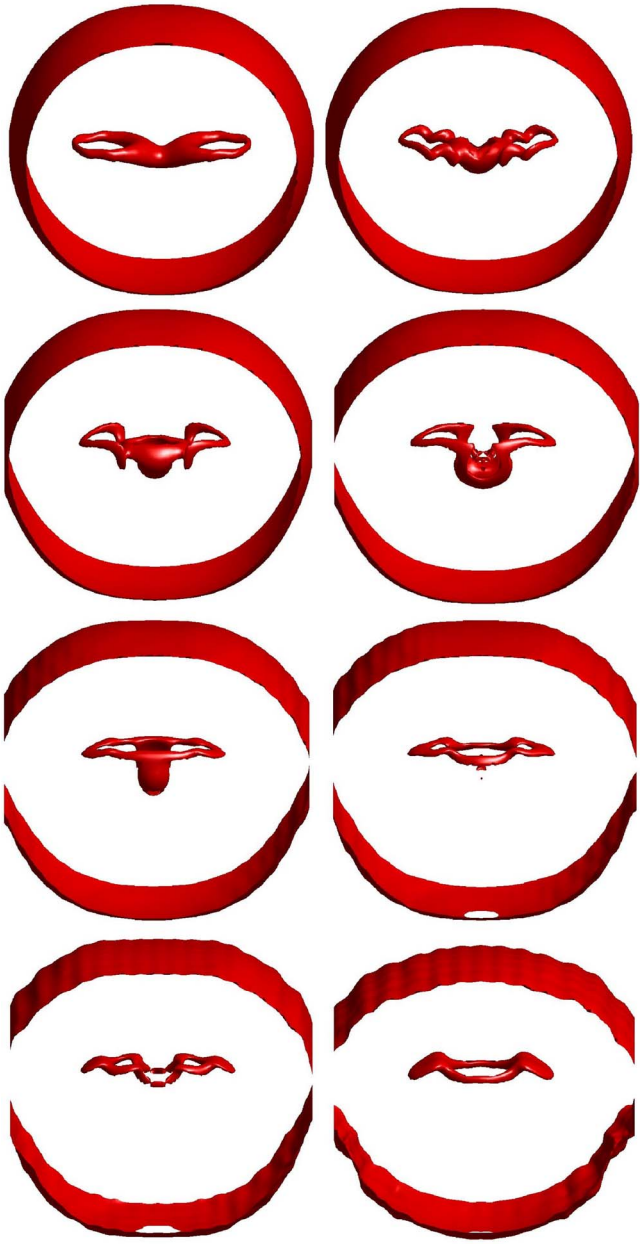

FIG. 3. (Color online) The same system as in Fig. 2, but the initial state of the real time evolution was obtained by means of propagating the wave functions in imaginary time for $t\omega=0.02$. The resulting reconnection process is more violent than the one displayed in Fig. 2. We show the isosurface plots at times $t\omega=0.1$, 0.2, 0.3, 0.4, 0.5, 0.6, 0.8, and 1.0.

In Figs. 2 and 3 the vortex rings are attracted to each other as their motion is also bent downwards. It should be emphasized that in the two-component BEC the vortex rings are initially static, there is no thermal atom component, and, after the preparation of the initial state, the dynamics is purely Hamiltonian with conserved total energy and no added dissipation term. In order for vortex rings to merge, they need to lose energy. In Figs. 4 and 5 we can clearly identify the released excess energy as sound, radiated outwards, and transformed into surface excitations. It is the turbulent dynamics triggered by the reconnection process which locally

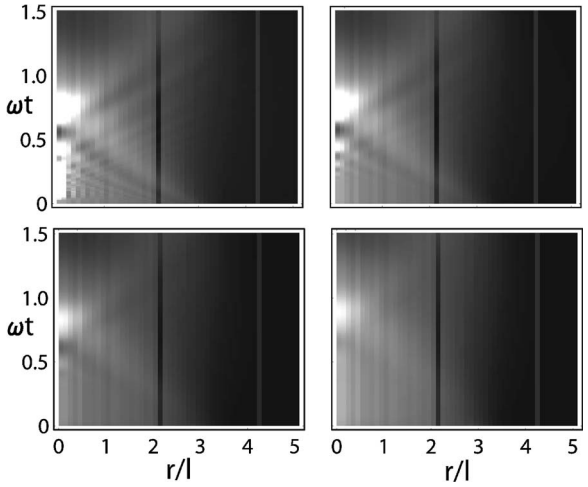

FIG. 4. The BEC energy density $\epsilon_t(r,t)$ averaged over the spherical angles during the reconnection process. The initial imaginary time evolution $\omega t=0$ (top left), $\omega t=0.02$ (top right), $\omega t=0.06$ (bottom left), and $\omega t=0.1$ (bottom right). The white color indicates a high value of the energy density. The sound waves first propagate towards the trap center when the vortex cusp is generated as the two rings merge. The energy is then radiated outwards and is transformed to surface excitations. The straight vertical stripes are an artifact of the numerical averaging procedure over the spherical angles.

produce an effective dissipation mechanism for the vortex configuration to relax. We can enhance the sound emission and the reconnection dynamics by considering a more rapid imprinting process. It is interesting to compare the merging vortex rings to the formation of a vortex lattice in a rotating BEC. In the latter case turbulent dynamics are triggered by the rotating potential and the vortex lattice can locally relax in the classical mean-field dynamics, even at $T=0$ and without any explicit damping term [2].

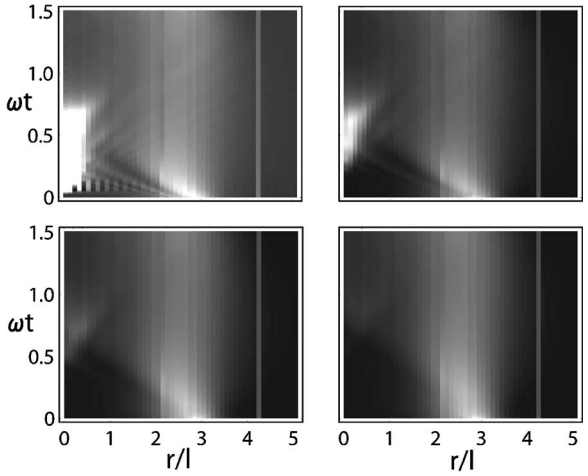

FIG. 5. The energy density $\epsilon_1(r,t)$ averaged over the spherical angles, depending only on the density of the BEC component containing the vortex ring. We show the same cases as in Fig. 4. In the second and the third figure one may clearly recognize the energy of the emitted sound pulses in the fifth and the sixth images of Figs. 2 and 3.

The reconnection process in Fig. 4 begins with a significant concentration of energy towards the trap center, as energy is propagated towards $r=0$. The vortex motion and the vortex reconnection process excite kelvin modes, resulting in a gradually decreasing vortex line length. The kelvin mode excitations of the vortex cores are clearly observable in the first snapshot images of Figs. 2 and 3. The generated vortex cusp at the reconnection region detaches from the merging vortex rings and is emitted as sound radiation. In the process the vortex energy is converted into a sound pulse which propagates away from the vortex. We observe large emission of vortex rings and/or rarefaction waves [54] at the reconnection region, e.g., in Fig. 2 at time $t\omega=0.6$ and in Fig. 2 around $0.5\leqslant t\omega\leqslant 0.6$. The emission events can also be seen in Fig. 5 as high energy regions close to the origin. The emitted sound energy results in strong surface excitations of the BEC (displayed in the last two images of Figs. 2 and 3 with the fastest sound pulses (shortest wavelength phonons) reaching the surface first.

IV. USING ULTRASLOW LIGHT IN THE STUDIES OF VORTEX COLLISIONS

We now turn our attention to an alternative method of vortex engineering, the light roadblock [6], which relies on imprinting density rather than phase modulations. In this study, we consider a two-dimensional geometry, where the vortices act as point particles, and consider the creation and subsequent interaction of multiple vortices. Due to the absence of absorption in the EIT, light is able to propagate in a sufficiently narrow geometry. We propose a method of using the light roadblock to create in a BEC two vortex pairs (two closely spaced vortices of opposite charge), which will collide and exhibit interesting dissipative dynamics and annihilations, hitherto unobserved experimentally. To understand the behavior quantitatively, we present a numerical study of vortex pair collisions in a regime in which the dissipation becomes a dominant mechanism.

A. Dissipation in vortex pair collisions

One of the fascinating aspects of vortices in current BECs is the fact that the relatively small nonlinearity leads to many finite compressible effects. In geometries where the system is essentially two dimensional, due to tight confinement in one direction (we will label y here), vortices act as point particles. In an incompressible fluid, they are indestructible particles that interact via conservative potentials, moving always according to the velocity fields created by neighboring vortices. For example, two vortices of like charge will orbit each other at some constant radius, while oppositely charged vortices will form pairs which travel along straight lines maintaining the same distance d between them [15]. In either case, the velocities are inversely proportional to the distance to the neighboring vortices. However, when the distances between vortex pairs become comparable to the healing length (which is the characteristic size of vortex cores), this picture breaks down. For example, in the case of corotating vortices of like charge, the pair will emit sound radiation and slowly drift to larger distances, lowering their energy [55]. The radiation occurs due to acceleration of the vortices as they undergo circular motion. Finite compressibility effects have also been important in explaining discrepancies between experimental and theoretical descriptions in excitations of vortex lattices [56].

The dynamics of multiple vortex configurations, particularly ones containing vortices of both circulations, can be particularly rich. For example, scattering between vortex pairs has been studied [57] as well as the existence and behavior of solitonlike structures in 2D geometries, and how they can dynamically form from closely spaced vortex pairs [58]. Previous studies have emphasized small perturbations of vortex motion due to compressibility effects. The dissipation is analogous to the length shortening and sound emission which occurs with colliding rings in 3D geometries studied above and in Refs. [48,49]. When the dissipation is sufficiently strong, the vortex motion can be strongly affected and the qualitative behavior will change. However, this has not been studied extensively in 2D geometries, and such effects have yet to be observed experimentally. We will see how the light roadblock allows us to engineer vortex pair collisions where this dissipation is strong and annihilations result in certain regimes.

B. Ultraslow light propagation and the light roadblock

We briefly review here the method of the light roadblock, based on slow light, to create large amplitude, small wavelength excitations, and outline our modeling of this system. Slow light is based on EIT [10], a quantum interference effect that permits the propagation of light through an otherwise opaque medium. A coupling laser, resonant with some initially unoccupied hyperfine state $|2\rangle$ and an optically excited state $|3\rangle$, is used to create the interference resulting in transparency (vanishing resonant absorption), a very large dispersion, and ultraslow group velocity of a probe pulse, resonant with an initially occupied state $|1\rangle$ and $|3\rangle$. Probe light pulses have been slowed down and spatially compressed (compared to their free space propagation values) by up to eight orders of magnitude [7–9]. As the probe propagates through the BEC, it puts the atoms into spatially dependent superpositions of $|1\rangle$ and $|2\rangle$ with the relative phase and amplitude of the wave functions (the atomic coherence) reflecting the amplitude and phase pattern of the input probe. As we will see below, combining this technique in BECs with the recently developed experimental technique of the light roadblock [6], whereby a fast spatial variation of the coupling field is introduced, provides an efficient method of inducing phase singularities on matter waves.

Here we focus on the case of a strongly anisoptropic trap, leading to essentially 2D dynamics. In Ref. [6], the geometry was truly 3D and in Ref. [32] the 3D aspects of the resulting topological structures in a similar system were investigated. We specifically consider the BEC occupying two hyperfine levels $|1\rangle$ and $|2\rangle$. These are connected, respectively, to a common excited state $|3\rangle$ by orthogonally propagating, resonant laser fields: the $+z$ propagating probe Ω_{13} and $+y$ propagating coupling Ω_{23}, each of wavelength λ. The excited state

$|3\rangle$ decays at Γ, forming a Λ three-level structure. In the slowly varying envelope (SVE) approximation for the light fields Ω_{i3} (with the rapid phase rotation at the optical frequencies and optical wave numbers factored out) the Maxwell's equations read [59]

$$\left(\frac{\partial}{\partial z}+\frac{1}{c}\frac{\partial}{\partial t}\right)\Omega_{13}=-f_{13}\sigma N[\Omega_{13}|\psi_1|^2+\Omega_{23}\psi_1^*\psi_2 e^{-ik(z-y)}], \tag{20}$$

$$\left(\frac{\partial}{\partial y}+\frac{1}{c}\frac{\partial}{\partial t}\right)\Omega_{23}=-f_{23}\sigma N[\Omega_{23}|\psi_2|^2+\Omega_{13}\psi_2^*\psi_1 e^{ik(z-y)}]. \tag{21}$$

Here N is the initial total number of BEC atoms, $k=2\pi/\lambda$, f_{i3} are dimensionless oscillator strengths, and $\sigma\equiv 3\lambda^2/2\pi$ is the resonant cross section. In Eqs. (20) and (21) we have adiabatically eliminated ψ_3 by assuming that the dynamics of the internal atomic degrees of freedom and the light are much faster than the external dynamics [59,60]. The BEC wave functions ψ_1,ψ_2 evolve according to generalized GPEs:

$$i\hbar\,\dot{\psi}_i=\left(H_0+\sum_k \kappa_{ik}|\psi_k|^2\right)\psi_i-\frac{i\hbar}{\Gamma}[|\Omega_i|^2\psi_i+\Omega_i^*\Omega_j\psi_j e^{-ik(\epsilon_i-\epsilon_j)}], \tag{22}$$

where $i=1,2, j\neq i$ and $\epsilon_1=z, \epsilon_2=y$. The last term in Eq. (22) results in both coherent exchange between $|1\rangle,|2\rangle$ as well as absorption into $|3\rangle$. The phase factors assure that atoms coherently coupled into $|2\rangle$ experience a two-photon momentum recoil relative to the nearly stationary $|1\rangle$ component. In our model, atoms which populate $|3\rangle$ and then spontaneously emit are assumed to be lost from the BECs.

If one were to input a weak ($|\Omega_{13}|\ll|\Omega_{23}|$) free space pulse of some length L_z into a BEC, simultaneous solution of Eqs. (20) and (22) reveals that the pulse is compressed to a length $(V_g/c)L_z$, where the group velocity is $V_g=|\Omega_{23}|^2/\Gamma f_{13}\sigma N|\psi_1|^2$, as it propagates through the BEC. Any phase and amplitude features along the longitudinal direction are similarly compressed while the transverse features are unaffected. While the usual description of slow light propagation depends on the weak probe assumption ($|\Omega_{13}|\ll|\Omega_{23}|$), the basic transfer of amplitude and phase patterns works even when this assumption is not strictly satisfied [59].

Spatial modulation of the input coupling field along z is then used to vary the speed and length of slow light pulses as they propagate through the BEC. In Ref. [6] this variation was accomplished by using a razor blade to block the coupling field from the BEC in the $z>0$ region so near $z=0$ the coupling intensity quickly varied from some large value to zero. In this region, the probe beam is slowed to zero group velocity and the length becomes arbitrarily small. At the same time the probe to coupling intensity ratio becomes large in this region, and so the fraction of atoms coupled into $|2\rangle$ becomes large. The result is a very narrow, large amplitude, density defect in the original condensate internal state $|1\rangle$, with the atoms in this region coupled into the other stable internal state $|2\rangle$. Because of the large photon recoil in the orthogonal geometry, atoms transferred to $|2\rangle$ leave the defect region in $\lesssim 1$ ms, leaving an empty hole in a single component BEC. This method is particularly useful for inducing density features in BECs smaller than the experimental optical resolution of the system, as the spatial compression at the roadblock occurs due to the slow light propagation effects and not focusing. This is particularly valuable in creating topological defects, since their characteristic length scale, the healing length, is typically <1 μm. Numerical simulation of the ^{23}Na experiment in Ref. [6] indicates that density defects~ 2 μm long (and nearly 100% depth) were being created even though the spatial variation of the coupling field (which *is* limited by optical resolution) was about ~ 10 μm. This interpretation was further supported by the fact that the density defects of the features were unobservable in in-trap absorption images but were clearly visible after 1 ms of free expansion.

C. Inducing vortex pair collisions with a light roadblock

In the original experiment [6] the imprinted density defects were seen to subsequently break up into a series of a solitons, due to the superfluid analog of shock waves. These solitons, in turn, broke up into pairs of vortices via the snake instability [11–13]. We now use our model to see how these pairs of vortices will collide with each other, providing a system in which to observe dissipative vortex dynamics.

We show an example of how this comes about in Fig. 6. In this example we consider a BEC with repulsive interactions in a trap with much stronger confinement along the y axis, with the trap frequencies satisfying $\omega_y\gg\omega_x,\omega_z$, so that the 2D limit of the GPE is valid. We assume that the defect has been created using the light roadblock technique, as explained earlier. Moreover, after the light fields have been turned off, we assume that the BEC component $|2\rangle$, which is initially filling the density defect in $|1\rangle$, is instantaneously coupled out of the trap due to the photon-induced recoil, as in the original experiments [6]. Then the BEC dynamics approximately follows from the single-component 2D GPE for $\tilde{\psi}(x,z)$, when we write $\psi_1(\mathbf{r})\simeq\phi(y)\tilde{\psi}(x,z)$, in terms of the ground state harmonic oscillator wave function $\phi(y)$ along the y axis:

$$i\hbar\frac{\partial\tilde{\psi}}{\partial t}=\left[-\frac{\hbar^2}{2m}\nabla^2+\frac{m}{2}(\omega_z^2z^2+\omega_x^2x^2)+\kappa_{2D}|\tilde{\psi}|^2\right]\tilde{\psi}, \tag{23}$$

where $\kappa_{2D}=\kappa_{11}/l_y\sqrt{2\pi}$, with $l_y=\sqrt{\hbar/m\omega_y}$. The additional density-dependent contribution to the scattering length in 2D is negligible when $\sqrt{2\pi}l_y/a\gg\ln(8\pi^{3/2}l_y n_{2D}a)$ [61], where $n_{2D}=N|\tilde{\psi}|^2$ denotes the 2D density. In the numerics, we choose $\omega_x/\omega_z\simeq 3.81$ and the nonlinearity $\kappa_{2D}=2360\hbar\omega_z l_z^2$ ($l_z=\sqrt{\hbar/m\omega_z}$). The numerical results depend on the dimensionless nonlinearity $\bar{\kappa}_{2D}\equiv\kappa_{2D}/\hbar\omega_z l_z^2=2\sqrt{2\pi}Na/l_y$, so our results are unchanged in any rescaling of the parameters which maintains constant Na/l_y and l_z/l_x, provided that the y confinement remains large enough for the 2D GPE (23) to be valid.

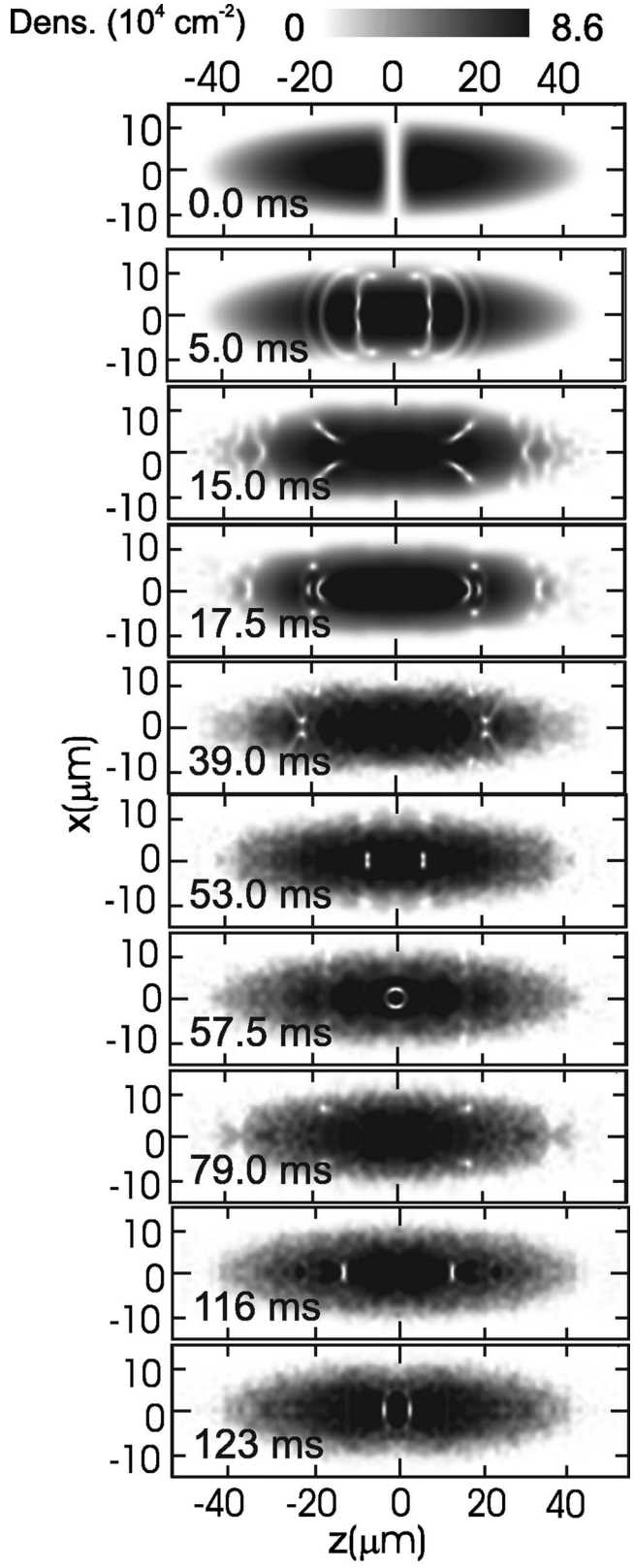

FIG. 6. The evolution of a 3 μm ($1/e$ half-width), full depth defect in a sodium BEC at the times indicated. Qualitative features of the evolution are explained in the text. The density scale refers to the normalized 2D density $|\tilde{\psi}(x,z)|^2$.

We then remove atoms from the relaxed ground state to create a narrow ($\sim 0.7 l_z$ half width) density hole, with 100% of the density removed along the central $z=0$ axis. The GPE (23) was propagated with a Crank-Nicholson algorithm with an equal spaced grid (300 points in x and 600 in z), with time steps $1.65\times 10^{-7}/\omega_z$. Both were varied to assure the results were not effected.

To make the connection with experimental parameters, we quote our results in terms of ^{23}Na parameters, which have a scattering length $a \simeq 2.75$ nm, and choose a trap $\omega_z = 2\pi \times 21$ Hz, giving $l_z \simeq 4.6$ μm and defect size ~ 3 μm. The ground state BEC in this trap has a central peak density of $n_{3D} = 1.5\times 10^{-14}$ cm^{-3} and the superfluid healing length at the cloud center is $\zeta \sim \hbar/(2m\kappa_{2D}|\tilde{\psi}|^2)^{1/2} \simeq 0.4$ μm.

In the limit of small amplitude and large wavelength, the imprinted defect would split into two counter-propagating sound waves [62]. However, due to the nonlinearity of the excitation (and the small length scale) [6] it here sheds off a series of a gray solitons [63], as seen in the snapshot at 5 ms. In addition, the slowest, and deepest soliton has begun to curl due to the snake instability, and vortices have begun to form. Because angular momentum is not being imparted to the system, vortices are formed in pairs of opposite charge. Investigation of the phase shows that all the vortices formed are singly quantized.

At 15 ms each quadrant contains a line of three vortices (alternating in the sign along each line). Note that here they are closely spaced so their density profiles overlap, and the identification of the vortices is done by finding singularities in the phase profile. Each vortex induces a circular velocity field about it, with the magnitude falling off as the inverse of the distance from the vortex center, and the direction is determined by its charge. The motion of each vortex is governed by the velocity field of the condensate, which is typically dominated by the velocity field induced by nearby vortices. In our example, this causes each of these lines to spin in pin-wheel fashion. In the 17.5 ms frame, this motion has induced collisions between pairs of vortices (from $x>0$ and $x<0$), resulting in annihilation of the vortices, with the energy carried off in sound waves, (seen as curved density defects) which quickly propagate towards the condensate edge and break up. What remains are four vortices, as seen at 39 ms. At 53 ms these vortices form two vortex pairs, that, due to the small distance between each pair, move very quickly towards the condensate center, on a collision course. Upon close approach with the other pair, the vortices make very sudden 90 degree turns and switch partners. Associated with this collision is a rather noticeable sound pulse resulting in a ringlike shape, seen at 57.5 ms. However, the four vortices survive and due to their interaction with the BEC edge, are sent around the edge of the BEC (79 ms) and eventually back along the same collision course (116 ms). This time the pairs are so close together that their density profiles greatly overlap (compared with the first approach, 53 ms). Upon the second collision, at 122 ms, rather than make the 90° turn, the vortices are destroyed (no phase singularities are visible after the collision) and the density defects propagate through each other and continue along the z axis (123 ms).

This sequence of vortex dynamics demonstrates a myriad of interesting features associated with the finite compressibil-

ity of the superfluid. In the limit of no compressibility, there is no sound emission and the vortex dynamics are completely conservative. In the absence of effects associated with the background condensate density, a vortex pair collision would look much like the collision at 57.5 ms, but with no associated sound emission, and with the size of the outgoing vortex pairs d (at 57.5 ms), the same as the incoming size (53.0 ms). However, due to the finite speed of sound, the vortices can exchange energy with phonons, dissipating some of their energy, as in the first collision of pairs at 57 ms, and in some cases annihilating, as in the second collision at 122 ms. In fact, the dissipation experienced during the first collision is what ultimately lowered the energy of each vortex pair, causing the pairs to be even smaller as they entered the second collision.

We note that the number of vortices created with the light roadblock and their subsequent dynamics can be controlled both by the size of the defect (which is ultimately controlled by the number of photons in the input probe pulse) and anisotropy in the x-z plane. For example, in Ref. [14] it was shown how a more circular shaped BEC leads to the production of many more vortices in each soliton. This geometry would be more favorable for minimizing effects due to BEC density variations. A sufficiently elongated trap would produce only two vortices per soliton, and may be more useful for tightly controlling the vortex trajectories and thus ensuring that a direct collision is induced.

D. Numerical study of dissipation in vortex pair collisions

To study this collision induced dissipation more systematically, we performed a series of numerical calculations of vortex pair collisions in a homogenous BEC. This was accomplished by first relaxing a condensate in a trap consisting of a large square flat potential surrounded by steep trapping walls. The product of the homogenous normalized 2D density and the nonlinearity $\kappa_{2D}|\tilde{\psi}^{(0)}|^2$ determine the characteristic length scale (the healing length) $\zeta \simeq \hbar/(2m\kappa_{2D}|\tilde{\psi}^{(0)}|^2)^{1/2}$, speed of sound $c_0=(\kappa_{2D}|\tilde{\psi}^{(0)}|^2/m)^{1/2}$, and time scale $t_0=\hbar/\kappa_{2D}|\tilde{\psi}^{(0)}|^2$. The 2D GPE (23) can then be renormalized into dimensionless form and we quote our results for this section in these units. Our homogenous trap region was chosen by $78\zeta\times 78\zeta$, and for numerical calculations, the trap was broken up into a grid with spacing 0.21ζ. Because the system is much larger than the vortex spacings we expect ζ to be the only important physical scale in the problem.

After relaxation we then impose four vortices: positive charge ones (clockwise velocity circulation) at $(x=7.4\zeta, z=14.7\zeta)$ and $(-7.4\zeta,-14.7\zeta)$ and negative ones at $(-7.4\zeta,14.7\zeta)$ and $(7.4\zeta,-14.7\zeta)$. In each case we impose the $e^{\pm i\phi}$ phase and a numerical estimate for the density profile [15]. This configuration is then relaxed further. As it relaxes, each vortex pair shrinks (i.e., the vortices drift towards $x=0$ and towards each other); bringing vortices of opposite charges together lowers the overall energy. We then stop this relaxation at various times and begin a real time evolution of the GPE. The circulations of the vortices are such that the pairs move towards each other and collide. In this way we can systematically study how vortex pairs of various initial sizes d_{in} act upon collision. For both relaxation and propagation of the GPE we used a Crank-Nicholson algorithm, with time steps $0.01t_0$.

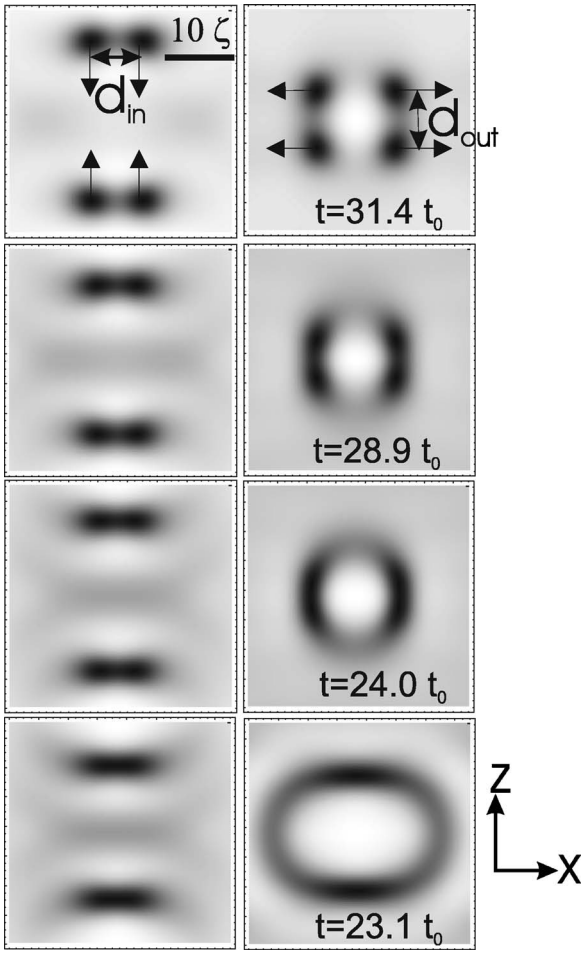

FIG. 7. Examples of vortex pair collisions, with each row showing two snapshots of a separate simulation with different initial pair distances d_{in}. Note that here white indicates high density (in contrast to Fig. 6). The left (right) hand column shows the vortices before (after) the collision of the pair. The initial distances of the pairs are, from top to bottom, $d_{\text{in}}/\zeta=7.0$, 5.4, 4.6, and 3.3. The arrows in the top row indicate the vortex direction.

Several examples of collisions are shown in Fig. 7. In the top example, $d_{\text{in}}=7.0\zeta$ and the vortices travel along the paths indicated by the arrows. Upon collision the vortices turn 90° and switch partners. There is barely a perceptible sound wave upon the collision. This sound radiation is due to the sudden acceleration experienced by the collision. In the second row $d_{\text{in}}=5.4\zeta$, and a noticeably larger sound wave is generated (due to the larger acceleration experienced by a smaller, and therefore faster, pair). Even though the density profiles of the pairs significantly overlap, the phase singularities remain in the wave function ψ_1 after the collision as the vortices travel out. This example is analogous to the first collision in Fig. 6 (57 ms). In the third row, $d_{\text{in}}=4.6\zeta$. In this case, the sound wave is bigger still, and the outgoing vortices

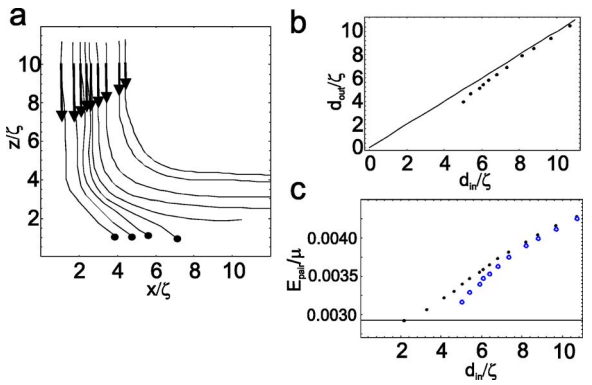

FIG. 8. (Color online) (a) The trajectories (specifically of the phase singularities) followed by the upper-right vortex for several different input sizes d_{in}. The arrow lengths are proportional to the observed velocity of the pairs at $z=10\zeta$ (with the longest arrow corresponding to $0.48c_0$). In four of the cases the vortices annihilated at the locations indicated with the dots. In the other cases, the phase singularities survived the collision. (b) For a series of cases, we plot the incoming pair size d_{in} (calculated when they are at $z=\pm 10\zeta$) versus the outgoing size d_{in} (when they reach $x=\pm 10\zeta$). (c) The energy of the vortex pairs versus the input distance d (black dots), calculated by taking half the energy of the two vortex pair configuration above the ground state energy. The horizontal line indicates the point at which the phase singularities disappear. The open circles (blue) then indicate the pair energies, calculated via the observed d_{out}.

have completely merged. Examining the phase indicates also that the phase singularities annihilate shortly after the collision. These structures bear resemblance to the "lumps" studied in [58]. In the bottom case, $d_{\mathrm{in}}=3.3\zeta$, the vortices annihilate early on in the collision, before the trajectories of the vortices have been significantly altered, and the remaining density waves simply pass through each other. This is similar to what happened in the second collision of Fig. 6 (122 ms).

It is interesting to observe how the sound wave energy emission pattern is strikingly different between the third and fourth cases of Fig. 7, with the energy emission primarily horizontal in the former and vertical in the latter. During the collision, sound is constantly emitted, but the majority of the energy is released at the moment of annihilation. In the former case, the annihilation occurs after the vortices have made a nearly 90° turn and the residual energy propagates in this direction. In the latter case, the annihilation occurs before a significant change in direction, thus sending most of the energy away in the original (vertical) direction. We also observed an intermediate case ($d_{\mathrm{in}}=4.2\zeta$), in which the sound energy propagated away with near perfect cylindrical symmetry.

In Fig. 8(a) we plot a series of trajectories followed by the vortices during these pair collisions (due to the symmetry, we only plot the vortex in the $x>0, z>0$ quadrant in each case). Initially all are following a trajectory almost purely in the $-z$ direction, with velocities proportional to the arrow lengths in the figure. The input size of the vortex pairs d_{in} is twice the initial x position. For sufficiently large vortex pairs $d \gg \zeta$ the velocity varies as $1/d$, in agreement with the theory of an incompressible fluid, however, as d becomes comparable to ζ the velocity begins to saturate, reaching a value $0.48c_0$ for the smallest pair we observed, $d_{\mathrm{in}}=2.18\zeta$. The phase singularities disappeared when the GP relaxed the vortex pair sizes smaller than this and became akin to 2D-soliton structures [58]. As each vortex approaches the counter-propagating pair near the origin, it begins to feel the pair's influence and turn to the $+x$ direction, eventually forming a new pair with its counterpart in the other pair. Again, for $d_{\mathrm{in}} \gg \zeta$ vortices, the system is conservative and the new vortex pairs propagate out with the same size $d_{\mathrm{out}}=d_{\mathrm{in}}$. However, as we saw in Fig. 7, large sound waves emit energy for smaller vortex pairs, and as a result, the outgoing pairs have lower energy and thus $d_{\mathrm{out}}<d_{\mathrm{in}}$. The outgoing versus incoming sizes are plotted for a series of cases in Fig. 8(b) and the trend towards more dissipation for smaller d_{in} is clearly seen. For the four smallest d_{in} plotted in Fig. 8(a), the dissipation is sufficient to induce an annihilation event at the locations indicated by the dots [thus these cases are not plotted in Fig. 8(b)].

Since the fundamental mechanism here is energy dissipation via sound emission, it is useful to analyze the results from an energy point of view. The power dissipation from vortices is proportional to the acceleration squared. This follows from the equivalence of the GPE superfluid dynamics to (2+1)-dimensional electrodynamics, with vortices replaced by charges and sound by electromagnetic radiation [55,64,65] and can also be demonstrated numerically [66]. A rough estimate of the scale of the acceleration can be obtained in the incompressible limit. The incoming velocity is $v_{\mathrm{in}} \sim c_0\zeta/d_{\mathrm{in}}$ and, due to the 90° turn this sets a scale for the total velocity change. The time of the interaction (the time during which acceleration is taking place) will be roughly $d_{\mathrm{in}}/v_{\mathrm{in}}$. Combining these considerations we estimate the time integration of the acceleration squared to be $\sim \zeta^3 c_0^3/d_{\mathrm{in}}^4$, thus we expect a strong dependence of the energy dissipation on d_{in} once it is comparable to ζ. Meanwhile, the energy of a vortex pair appears as $\mu \ln(ad/\zeta)$, where a is a constant of order unity [15]. When the dissipation is large enough so that the outgoing pair size would be $d_{\mathrm{out}}<2.18\zeta$, the phase singularities will disappear during the collision. While this gives us an order of magnitude estimates, numerical analysis is required to get the correct coefficients and also because the incompressible results begin to break down in the interesting regime.

To calculate the energy dissipation in our results, we calculate the energy of our relaxed wave function at the beginning of each simulation. By subtracting from this the ground state energy (without vortices) and halving the result (since there are two vortex pairs), we obtain a vortex pair energy as a function of size $E_{\mathrm{pair}}(d)$. This quantity is plotted for each d_{in} as black dots in Fig. 8(c). The horizontal line indicates the point at which no phase singularity was observed ($d<2.18\zeta$). We then plot, using the observed outgoing size d_{out} and our numerically calculated energy dependence $E_{\mathrm{pair}}(d)$, the outgoing pair energy and plot it versus d_{in} as open circles. The difference between the dotted curve and the curve denoted by open circles thus indicates the energy carried off by phonons in each case. Fitting to the above expected dependence shows a dissipation rate $\beta\mu(\zeta^4/d_{\mathrm{in}}^4)$ with $\beta=0.0033$ but we note that a fit to a $1/d_{\mathrm{in}}^3$ behavior works

better (presumably because the scaling slightly changes as $d_{\mathrm{in}} \sim \zeta$). For the four smallest incoming pairs, the energy dissipation was large enough so that the pair energy fell below the horizontal line and the vortex phase singularity was eliminated. Because ζ is the defining scale in the problem, this threshold for annihilation $d_{\mathrm{in}} \approx 4\zeta$ should hold for any head-on collision of two vortex pairs. In general, the angle of collision will play a role in this threshold.

V. CONCLUSIONS

We investigated methods for imprinting desired patterns of phase singularities on atomic matter waves by means of em fields inducing transitions between different hyperfine levels of the atom as well as by means of controlling the ultraslow light propagation inside the atomic cloud. By appropriate field superpositions one may construct phase singularities around the node points of the em field amplitude which can then be imprinted on the BECs using coherently driven atomic transitions. In particular, we showed that a simple superposition of two Gaussian laser beams, which exhibit a different beam waist, is sufficient to imprint a phase singularity forming a closed circular loop with a 2π phase winding around the loop. This provides a controlled method of creating vortex rings on atomic superfluids, where the size, the position, and the orientation of the ring can be engineered by modifying the parameters of the beam superposition. Moreover, we showed that the imprinting techniques can be generalized for imprinting vortex ring pairs and multivortex systems which are especially interesting in the studies of vortex reconnections. The experimental technology of diffractive optical components, such as optical holograms, may be particularly useful in generating the light beams with the desired phase and the amplitude profiles. We investigated in detail one specific example of vortex reconnections resulting from the imprinted phase profile by considering two merging vortex rings in a trapped, two-component atomic BEC. We used the parameters of ^{87}Rb experiments and calculated the energy distribution in the atom cloud during the reconnection process.

In addition to direct imprinting of phase singularities on the BECs, we also explored the recently developed experimental technique of preparing defects by means of abruptly distorting the ultraslow light propagation in atomic BECs with light roadblocks. We showed that in a tightly confined 2D configuration this technique is particularly useful in the studies of point vortex collisions. Similarly to the reconnection dynamics of the vortex rings in an isotropic trap, we explored the role of sound emission in the collision processes of the point vortices and showed how the binding energy of the pair can be dissipated during close range collisions. Sufficiently large energy dissipation leads to the interesting phenomenon of vortex annihilation.

Our results point the way towards a number of experiments that can be implemented with present day cold-atom and laser technology, and that could allow controlled experimental investigation of complicated vortex interactions.

ACKNOWLEDGMENTS

J.R. acknowledges discussions with James Anglin and Mark Dennis and financial support from the EPSRC and NSF through a grant for the Institute for Theoretical Atomic, Molecular and Optical Physics at Harvard University and Smithsonian Astrophysical Observatory. Z.D. acknowledges NIST Gaithersburg, where some of this work was carried out, and discussions there with Jamie Williams.

[1] R. J. Donnelly, *Quantized Vortices in Helium II* (Cambridge University Press, Cambridge, 1991).
[2] C. Lobo, A. Sinatra, and Y. Castin, Phys. Rev. Lett. **92**, 020403 (2004).
[3] J. Ruostekoski and J. R. Anglin, Phys. Rev. Lett. **86**, 3934 (2001).
[4] C. M. Savage and J. Ruostekoski, Phys. Rev. A **68**, 043604 (2003); J. Ruostekoski, *ibid.* **70**, 041601(R) (2004).
[5] R. A. Battye, N. R. Cooper, and P. M. Sutcliffe, Phys. Rev. Lett. **88**, 080401 (2002).
[6] Z. Dutton, M. Budde, C. Slowe, and L. V. Hau, Science **293**, 663 (2001).
[7] L. V. Hau, S. E. Harris, Z. Dutton, and C. H. Behroozi, Nature (London) **397**, 594 (1999).
[8] M. M. Kash, V. A. Sautenkov, A. S. Zibrov, L. Hollberg, G. R. Welch, M. D. Lukin, Y. Rostovtsev, E. S. Fry, and M. O. Scully, Phys. Rev. Lett. **82**, 5229 (1999).
[9] D. Budker, D. F. Kimball, S. M. Rochester, and V. V. Yashchuk, Phys. Rev. Lett. **83**, 1767 (1999).
[10] S. E. Harris, Phys. Today **50**(7), 36 (1997).
[11] B. B. Kadomstev and V. I. Petviashvili, Sov. Phys. Dokl. **15**, 539 (1970).
[12] D. L. Feder, M. S. Pindzola, L. A. Collins, B. I. Schneider, and C. W. Clark, Phys. Rev. A **62**, 053606 (2000).
[13] B. P. Anderson, P. C. Haljan, C. A. Regal, D. L. Feder, L. A. Collins, C. W. Clark, and E. A. Cornell, Phys. Rev. Lett. **86**, 2926 (2001).
[14] Z. Dutton, N. S. Ginsberg, C. Slowe, and L. V. Hau, Europhysics News, **35**, 33 (2004).
[15] A. L. Fetter in *Bose-Einstein Condensates in Atomic Gases*, edited by M. Inguscio, S. Stringari, and C. Wieman, *Proceedings of the International School of Physics Enrico Fermi*, Course CXL (International Organisations Services B.V., Amsterdam, 1999), p. 201.
[16] J. R. Anglin and W. Ketterle, Nature (London) **416**, 211 (2002).
[17] E. L. Bolda and D. F. Walls, Phys. Lett. A **246**, 32 (1998).
[18] K.-P. Marzlin, W. Zhang, and E. M. Wright, Phys. Rev. Lett. **79**, 4728 (1997).
[19] R. Dum, J. I. Cirac, M. Lewenstein, and P. Zoller, Phys. Rev. Lett. **80**, 2972 (1998).
[20] L. Dobrek, M. Gajda, M. Lewenstein, K. Sengstock, G. Birkl, and W. Ertmer, Phys. Rev. A **60**, R3381 (1999).
[21] J. E. Williams and M. J. Holland, Nature (London) **401**, 568

(1999).
[22] J. Ruostekoski, Phys. Rev. A **61**, 041603(R) (2000).
[23] H. Pu, S. Raghavan, and N. P. Bigelow, Phys. Rev. A **63**, 063603 (2001).
[24] T. Isoshima, M. Nakahara, T. Ohmi, and K. Machida, Phys. Rev. A **61**, 063610 (2000).
[25] Z. Dutton and J. Ruostekoski, Phys. Rev. Lett. **93**, 193602 (2004).
[26] M. R. Matthews, B. P. Anderson, P. C. Haljan, D. S. Hall, C. E. Wieman, and E. A. Cornell, Phys. Rev. Lett. **83**, 2498 (1999).
[27] A. E. Leanhardt, A. Görlitz, A. P. Chikkatur, D. Kielpinski, Y. Shin, D. E. Pritchard, and W. Ketterle, Phys. Rev. Lett. **89**, 190403 (2002).
[28] A. E. Leanhardt, Y. Shin, D. Kielpinski, D. E. Pritchard, and W. Ketterle, Phys. Rev. Lett. **90**, 140403 (2003).
[29] Y. Shin, M. Saba, M. Vengalattore, T. A. Pasquini, C. Sanner, A. E. Leanhardt, M. Prentiss, D. E. Pritchard, and W. Ketterle, Phys. Rev. Lett. **93**, 160406 (2004).
[30] S. Burger, K. Bongs, S. Dettmer, W. Ertmer, K. Sengstock, A. Sanpera, G. V. Shlyapnikov, and M. Lewenstein, Phys. Rev. Lett. **83**, 5198 (1999).
[31] J. Denschlag *et al.*, Science **287**, 97 (2000).
[32] N. S. Ginsberg, J. Brand, and L. V. Hau, Phys. Rev. Lett. **94**, 040403 (2005).
[33] J. Ruostekoski and J. R. Anglin, Phys. Rev. Lett. **91**, 190402 (2003).
[34] C. Liu, Z. Dutton, C. H. Behroozi, and L. V. Hau, Nature (London) **409**, 490 (2001).
[35] D. F. Phillips, A. Fleischhauer, A. Mair, R. L. Walsworth, and M. D. Lukin, Phys. Rev. Lett. **86**, 783 (2001).
[36] M. Fleischhauer and M. D. Lukin, Phys. Rev. Lett. **84**, 5094 (2000).
[37] Ö. E. Müstecapliioglu and M. Ö. Oktel, Phys. Rev. Lett. **94**, 220404 (2005).
[38] D. S. Hall, M. R. Matthews, J. R. Ensher, C. E. Wieman, and E. A. Cornell, Phys. Rev. Lett. **81**, 1539 (1998).
[39] R. Dumke, T. Müther, M. Volk, W. Ertmer, and G. Birkl, Phys. Rev. Lett. **89**, 220402 (2002).
[40] J. Leach, M. R. Dennis, J. Courtial, and M. J. Padgett, Nature (London) **432**, 165 (2004).
[41] J. Leach, M. R. Dennis, J. Courtial, and M. J. Padgett, New J. Phys. **7**, 55 (2005).
[42] M. V. Berry and M. R. Dennis, Proc. R. Soc. London, Ser. A **457**, 2251 (2001).
[43] M. V. Berry and M. R. Dennis, J. Phys. A **34**, 8877 (2001).
[44] C. Bäuerle, V. M. Bunkov, S. N. Fisher, H. Godfrin, and G. R. Pickett, Nature (London) **382**, 332 (1996); V. M. H. Ruutu, V. B. Eltsov, A. J. Gill, T. W. B. Kibble, M. Krusius, Y. G. Makhlin, B. Placais, G. E. Volovik, and W. Xu, *ibid.* **382**, 334 (1996).
[45] W. F. Vinen, Phys. Rev. B **61**, 1410 (2000).
[46] J. Koplik and H. Levine, Phys. Rev. Lett. **71**, 1375 (1993).
[47] N. G. Berloff and P. H. Roberts, J. Phys. A **34**, 10057 (2001).
[48] J. Koplik and H. Levine, Phys. Rev. Lett. **76**, 4745 (1996).
[49] M. Leadbeater, T. Winiecki, D. C. Samuels, C. F. Barenghi, and C. S. Adams, Phys. Rev. Lett. **86**, 1410 (2001).
[50] H. Lamb, *Hydrodynamics* (Dover, New York, 1945).
[51] P. H. Roberts and J. Grant, J. Phys. A **4**, 55 (1971).
[52] M. Leadbeater, D. C. Samuels, C. F. Barenghi, and C. S. Adams, Phys. Rev. A **67**, 015601 (2003).
[53] J. Javanainen and J. Ruostekoski, cond-mat/0411154.
[54] N. G. Berloff, Phys. Rev. Lett. **94**, 120401 (2005).
[55] E. Lundh and P. Ao, Phys. Rev. A **61**, 063612 (2000).
[56] G. Baym, Phys. Rev. Lett. **91**, 110402 (2003).
[57] A. S. Kovalel, S. Homeneas, and F. G. Martens, Eur. Phys. J. B **25**, 89 (2002).
[58] G. Huang, V. A. Makarov, and M. G. Velarde, Phys. Rev. A **67**, 023604 (2003).
[59] Z. Dutton and L. Vestergaard Hau, Phys. Rev. A **70**, 053831 (2004).
[60] J. Javanainen and J. Ruostekoski, Phys. Rev. A **52**, 3033 (1995).
[61] D. S. Petrov, M. Holzmann, and G. V. Shlyapnikov, Phys. Rev. Lett. **84**, 2551 (2000).
[62] M. R. Andrews, D. M. Kurn, H. J. Miesner, D. S. Durfee, C. G. Townsend, S. Inouye, and W. Ketterle, Phys. Rev. Lett. **79**, 553 (1997).
[63] S. A. Morgan, R. J. Ballagh, and K. Burnett, Phys. Rev. A **55**, 4338 (1997).
[64] D. P. Arovas and J. A. Freire, Phys. Rev. B **55**, 1068 (1997).
[65] V. Ambegaokar, B. I. Halperin, D. R. Nelson, and E. D. Siggia, Phys. Rev. B **21**, 1806 (1980).
[66] N. G. Parker, N. P. Proukakis, C. F. Barenghi, and C. S. Adams, Phys. Rev. Lett. **92**, 160403 (2004).